Atmos. Chem. Phys. Discuss., 14, 31281–31317, 2014
www.atmos-chem-phys-discuss.net/14/31281/2014/
doi:10.5194/acpd-14-31281-2014

Atmospheric Chemistry and Physics Discussions

Atmospheric nitrogen oxides (NO and NO_2) at Dome C, East Antarctica, during the OPALE campaign

M. M. Frey[1], H. K. Roscoe[1], A. Kukui[2,3], J. Savarino[4,5], J. L. France[6], M. D. King[6], M. Legrand[4,5], and S. Preunkert[4,5]

[1]British Antarctic Survey, Natural Environment Research Council, Cambridge, UK
[2]Laboratoire Atmosphère, Milieux et Observations Spatiales (LATMOS), UMR8190, CNRS-Université de Versailles Saint Quentin, Université Pierre et Marie Curie, Paris, France
[3]Laboratoire de Physique et Chimie de l'Environnement et de l'Éspace (LPC2E), UMR6115 CNRS-Université d'Orléans, 45071 Orléans cedex 2, France
[4]Université Grenoble Alpes, Laboratoire de Glaciologie et Géophysique de l'Environnement (LGGE), 38000 Grenoble, France
[5]CNRS, Laboratoire de Glaciologie et Géophysique de l'Environnement (LGGE), 38000 Grenoble, France
[6]Department of Earth Sciences, Royal Holloway University of London, Egham, Surrey, TW20 0EX, UK

Received: 9 November 2014 – Accepted: 21 November 2014 – Published: 11 December 2014

Correspondence to: M. M. Frey (maey@bas.ac.uk)

Published by Copernicus Publications on behalf of the European Geosciences Union.

ACPD
14, 31281–31317, 2014

Abstract

Mixing ratios of the atmospheric nitrogen oxides NO and NO_2 were measured as part of the OPALE (Oxidant Production in Antarctic Lands & Export) campaign at Dome C, East Antarctica (75.1° S, 123.3° E, 3233 m), during December 2011 to January 2012. Profiles of NO_x mixing ratios of the lower 100 m of the atmosphere confirm that, in contrast to South Pole, air chemistry at Dome C is dominated by strong diurnal cycles in solar irradiance and atmospheric stability. Depth profiles of mixing ratios in firn air suggest that the upper snowpack at Dome C holds a significant reservoir of photolytically produced NO_2 and is a sink of gas phase ozone (O_3). First-time observations of BrO at Dome C suggest 2–3 pptv near the ground, with higher levels in the free troposphere. Assuming steady-state, observed mixing ratios of BrO and RO_2 radicals are too low to explain the large NO_2 : NO ratios found in ambient air. A previously not considered interference with pernitric acid (HNO_4) may explain part of this inconsistency. During 2011–2012 NO_x mixing ratios and flux were larger than in 2009–2010 consistent with also larger surface O_3 mixing ratios resulting from increased net O_3 production. Large NO_x mixing ratios arose from a combination of changes in mixing height and NO_x snow emission flux F_{NO_x}. During 23 December 2011–12 January 2012 median F_{NO_x} was twice that during the same period in 2009–2010 due to significantly larger atmospheric turbulence and a slightly stronger snowpack source. A tripling of F_{NO_x} in December 2011 was largely due to changes in snow pack source strength caused primarily by changes in NO_3^- concentrations in the snow skin layer, and only to a secondary order by decrease of total column O_3 and associated increase in NO_3^- photolysis rates. Systematic changes in the quantum yield of NO_3^- photolysis over time may contribute to the observed F_{NO_x} variability.

ACPD
14, 31281–31317, 2014

1 Introduction

The nitrogen oxides NO and NO_2 (NO_x = NO + NO_2) play a key role in the polar troposphere in determining its oxidation capacity, defined here as the sum of O_3, HO_x radicals, and hydrogen peroxide (H_2O_2). The influence is achieved via photolysis of NO_2, the only source for in situ production of tropospheric O_3, through shifting HO_x radical partitioning towards the hydroxyl radical (OH) via the reaction $NO + HO_2 \rightarrow NO_2 + OH$, and finally through reactions with peroxyradicals $NO + HO_2$ (or RO_2) which compete with the formation of peroxides (H_2O_2 and ROOH).

Atmospheric mixing ratios of NO_x in the atmospheric boundary layer of coastal Antarctica are small, with average NO_x values in summer not exceeding 30 pptv (Bauguitte et al., 2012). The build up of large mixing ratios is prevented by gas-phase formation of halogen nitrates (e.g. $BrNO_3$, INO_3) followed by their heterogeneous loss (Bauguitte et al., 2012). Conversely, mixing ratios of NO_x on the East Antarctic Plateau are unusually large, similar to those from the mid-latitudes (Davis et al., 2008; Slusher et al., 2010; Frey et al., 2013). Such large mixing ratios of NO_x were found to arise from a combination of several factors: continuous sunlight, location at the bottom of a large air drainage basin, low temperatures leading to low primary production rates of HO_x radicals, significant emissions of NO_x from surface snow, and a shallow boundary layer (Davis et al., 2008; Frey et al., 2013, and refs. therein).

Snow emissions of NO_x, observed at several polar locations (e.g. Jones et al., 2001; Honrath et al., 2000b), are driven by UV-photolysis of nitrate in snow (Honrath et al., 2000b; Simpson et al., 2002) and are now considered to be an essential component of air-snow cycling of oxidised nitrogen species above the polar ice sheets (Davis et al., 2008; Frey et al., 2009b) and likely also above mid-latitude snow packs (Honrath et al., 2000a; Fisher et al., 2005). Atmospheric dynamics, i.e. vertical mixing strength and mixing height, can explain some of the observed temporal variability and site-specific chemical composition of the lower troposphere at South Pole and Summit, Greenland (Cohen et al., 2007; Neff et al., 2008). Recently, the very strong diurnal cycle of mix-

ACPD
14, 31281–31317, 2014

ing ratios of NO_x observed at Dome C, East Antarctic Plateau, during summer was shown to result from the interplay between boundary layer mixing and emissions from the photochemical snow source; during calm periods a minimum of NO_x mixing ratios occurred around local noon and a maximum in the early evening coinciding with the development and collapse of a convective boundary layer (Frey et al., 2013). A key parameter of the physical atmospheric processes at play is the turbulent diffusivity of the atmosphere, which controls the mixing height, h_z, of the atmospheric boundary layer and contributes to the magnitude of the flux of trace chemical species emitted by the snow (e.g. Frey et al., 2013).

The impact of NO_x emissions from snow on the oxidation capacity of the lower troposphere in summer can be significant. For example, NO_x snow emissions can result in net ozone production as observed in the interior of Antarctica (Crawford et al., 2001; Legrand et al., 2009; Slusher et al., 2010) as well as unusually large mixing ratios of hydroxyl radical levels as detected at South Pole (Davis et al., 2008, and refs. therein). Furthermore, in Antarctica the gas phase production of hydrogen peroxide (H_2O_2), the only major atmospheric oxidant preserved in ice cores, is sensitive to NO released by the surface snowpack (e.g. Frey et al., 2005, 2009a). A steady-state analysis of ratios of NO_2 : NO at Dome C suggested that mixing ratios of peroxy radicals (not measured at the time) are possibly larger at Dome C than any previous observations in air above polar snow (Frey et al., 2013).

The quantitative understanding of emissions of NO_x from snow remains incomplete, but it is a research priority to be able to parameterise global models to assess for example global impacts of chemical air-snow exchange on tropospheric ozone (e.g. Zatko et al., 2013). Emissions of NO_x from snow at Dome C are among the largest observed above either polar ice sheet, but are typically underestimated by models, especially at large solar zenith angles (Frey et al., 2013). One significant model uncertainty is the quantum yield of nitrate photolysis in snow, which is related to the location of the nitrate ion in snow grains, and needs to be better constrained by observations (Frey et al., 2013; Meusinger et al., 2014).

ACPD
14, 31281–31317, 2014

The study presented here was part of the comprehensive atmospheric chemistry campaign OPALE (Oxidant Production and its Export from Antarctic Lands) in East Antarctica (Preunkert et al., 2012) and provided the opportunity to measure NO_x mixing ratios and flux during a second summer season, after a previous campaign in 2009–2010 (Frey et al., 2013). The study objectives were firstly to extend the existing data set with mixing ratio profiles of the lower atmosphere and the firn air (interstitial air) column of the upper snow pack. Secondly, to investigate if observed $NO_2 : NO$ ratios are consistent with measurements of hydroxyl and halogen radicals. And thirdly, to analyse the main drivers of the atmospheric NO_x emission flux from snow.

2 Methods

The measurement campaign of 50 days took place at Dome C (75.1° S, 123.3° E, 3233 m) from 23 November 2011 to 12 January 2012. Similar to the 2009–2010 campaign atmospheric sampling was performed from an electrically heated lab shelter (Weatherhaven tent) located in the designated clean-air sector 0.7 km upwind (South) of Concordia station (see map in Frey et al., 2013). All times are given as local time (LT), equivalent to UTC + 8 h, and during the study period the sun always remained above the horizon.

2.1 NO_x concentration and flux measurements

Three 20 m-long intake lines (Fluoroline 4200 high purity PFA, I.D. 4.0 mm) were mounted on a mast about 15 m into the prevailing wind to continuously sample air at 0.01, 1.00 and 4.00 m above the natural snow pack. The intake lines were away from the influence of the drifted snow around the lab shelter. On 9 January 2012 vertical profiles of the lower atmosphere were sampled by attaching a 100 m-long intake line to a helium-filled weather balloon, which was then manually raised and lowered. During selected time periods firn air was sampled, to depths 5–100 cm, by means of a cus-

ACPD
14, 31281–31317, 2014

tom built probe. The probe consisted of a tube (10 cm diameter) which was lowered vertically into a pre-cored hole to the chosen snow depth, passing through a disc (1 m diameter) resting on the snow surface. The disk had a lip of 10 cm protruding into the snow. The lip and disk minimised preferential pumping of ambient air along the tube walls. The air intake was mounted at the bottom end of the vertical tube so that only air from the bottom and sides, using small horizontal holes, could enter. All probe components were made from UV-transparent plastic (Plexiglas Sunactive GS 2458). 2 × 3 m sheets of UV-opaque (Acrylite OP-3) and UV-transparent (Acrylite OP-4) plexiglass, mounted on aluminium frames at 1 m above the snow surface, were used to deduce the effect of UV radiation on the mixing ratio of NO_x in the interstitial air and avoid any temperature effect altering the snow surface.

To measure NO_x the same 2-channel chemiluminescence detector (CLD) and experimental set up as during the 2009–2010 campaign were used (instrument schematic in Frey et al., 2013). Channel one of the CLD measured atmospheric mixing ratios of NO whereas the other channel determined the sum of the mixing ratios of NO and NO originating from the quantitative photolytic conversion of NO_2. The difference between the two channels was used to calculate atmospheric mixing ratios of NO_2.

The CLD employed converts also nitrous acid (HONO) to NO in the photolytic converter and thus HONO sampled by the CLD is an interference, as discussed previously (Frey et al., 2013). Average mixing ratios of HONO at 1 m above the snowpack measured with the LOPAP (Long Path Absorption Photometer) technique were ∼ 35 pptv (Legrand et al., 2014). The corresponding downward correction for NO_2 at 1 m above the snowpack is ∼ 5 %. However the LOPAP technique may overestimate the mixing ratio of HONO owing to an interference with pernitric acid (HNO_4) (Legrand et al., 2014). True corrections of NO_2 inferred from modelled HONO mixing ratios (Legrand et al., 2014) are more likely to be on the order of < 1.5 %. Due to the uncertainty in absolute mixing ratios of HONO, no correction of NO_x values for the HONO interference was applied.

ACPD
14, 31281–31317, 2014

The presence of strong gradients in mixing ratios of HONO inferred by Legrand et al. (2014) can potentially lead to an overestimate of NO_x concentration differences between 0.01 and 1.0 m used below to derive the vertical NO_x flux. During the OPALE campaign the atmospheric life time of NO_x, τ_{NO_x}, ranged between 3 h (12:00 LT) and 7 h (00:00 LT), whereas that of HONO, τ_{HONO}, ranged between 4.5 min (12:00 LT) and 24 min (00:00 LT) (Legrand et al., 2014). The life time of HONO is comparable to the typical transport times of ∼ 10 min between the surface and 1 m at Dome C in summer (Frey et al., 2013). Hence, HONO : NO_x ratios as well as corresponding corrections required for NO_2 are not constant with height above the snow surface. No gradients of HONO mixing ratios were measured but modelled values were 18.8 and 10.2 pptv at noon, and 15.3 and 12 pptv at midnight, at 0.1 and 1.0 m, respectively (Legrand et al., 2014). Corresponding corrections of mean NO_2 mixing ratios for HONO are 1.3–1.5 % with a maximum difference of 0.2 % between 0.1 and 1.0 m. Thus, at Dome C a strong gradient in the mixing ratios of HONO was a negligible effect on the mixing ratios of NO_x measured at 0.1 and 1.0 m and thus a negligible effect on the estimated NO_x flux.

The thermal decomposition of HNO_4 in the sample lines or photolytic converter of the CLD could also cause a positive bias of NO_x. Spike tests showed that the sample air residence time in the total volume of inlets and CLD is ∼ 4 s (Frey et al., 2013). At a sample flow rate of 5.0 STP – L min^{-1} the residence time in the combined volume of photolytic converter and CLD reaction cell is estimated to be < 2 s. Atmospheric lifetimes of HNO_4, τ_{HNO_4}, with respect to thermal decomposition to HO_2+NO_2 were calculated at mean ambient pressure (645 mb) using rate coefficients after Jacobson (1999). τ_{HNO_4} decreases from 8.6 h at mean ambient temperature assumed in the sample intake lines (−30 °C) to 7 s at the maximum observed temperature in the photolytic converter (30 °C). Therefore, NO_2 production from HNO_4 thermal decomposition is negligible in the sample intake lines, but approximately 25 % of all HNO_4 may be converted to NO_2 in the photolytic converter. A recent airborne campaign above the East Antarctic Plateau showed mean summertime atmospheric mixing ratios of HNO_4 between 0 and 50 m of 65 pptv with maxima about twice as large (Slusher et al., 2010). HNO_4 present

ACPD
14, 31281–31317, 2014

at these values could potentially produce 33–66 pptv of NO_2 in the photolytic converter equivalent to 16–32 % of the average NO_2 mixing ratio measured at 1 m. We attempted to test for the presence of HNO_4 by passing ambient air through a 50 m intake heated to 50 °C before it entered the CLD. However, during the tests no significant change in NO_2 was detected.

The turbulent flux of NO_x, F_{NO_x}, was estimated using the integrated flux gradient method (e.g. Lenschow, 1995) and mixing ratios of NO_x measured at 0.01 and 1.0 m. F_{NO_x} in the surface layer is parameterised according to the Monin–Obukhov similarity theory (MOST) whose predictions of flux-profile relationships at Halley, an Antarctic coastal site of the same latitude as DC, agree well with observations (Anderson and Neff, 2008, and references therein):

$$F_{NO_x} = -\frac{\kappa u_* z}{\Phi_h\left(\frac{z}{L}\right)}\frac{\partial c}{\partial z} \tag{1}$$

with the von Karman constant κ (set to 0.40), friction velocity u_*, height z, concentration gradient $\partial c/\partial z$, and $\Phi_h(\frac{z}{L})$ an empirically determined stability function for heat with L as the Monin–Obukhov length. Assuming constant flux across the layer between the two measurement heights z_1 and z_2 allows the integration to be solved and yields:

$$F_{NO_x} = -\frac{\int_{c_1}^{c_2}\kappa u_* \partial c}{\int_{z_1}^{z_2}\Phi_h\left(\frac{z}{L}\right)\frac{\partial z}{z}} = -\frac{\kappa u_*[c(z_2)-c(z_1)]}{\int_{z_1}^{z_2}\Phi_h\left(\frac{z}{L}\right)\frac{\partial z}{z}} \tag{2}$$

Stability functions Φ_h used are given in Frey et al. (2013), while their integrated forms can be found in Jacobson (1999). Friction velocity u_* and L were computed from the three-dimensional wind components (u, v, w) and temperature measured at 25 Hz by a sonic anemometer (Metek USA-1) mounted next to the uppermost NO_x intake line, at 4 m above the snow surface. Processing of raw data in 10 min blocks included temperature cross-wind correction and a double coordinate rotation to force mean w to zero (Kaimal and Finnigan, 1994; Van Dijk et al., 2006). Equation (2) implies that

ACPD
14, 31281–31317, 2014

a positive flux is in upward direction, equivalent to snow pack emissions and a negative flux is in downward direction, equivalent to deposition.

The application of MOST requires the following conditions to be met: (a) flux is constant between measurement heights z_1 and z_2, (b) the lower inlet height z_1 is well above the aerodynamic roughness length of the surface, (c) the upper inlet height z_2 is within the surface layer, i.e. below 10 % of the boundary layer height h_z (Stull, 1988), and (d) z_1 and z_2 are far enough apart to allow for detection of a significant concentration difference $[c(z_2) - c(z_1)]$. During summer at Dome C conditions (a) and (b) are met as discussed in Frey et al. (2013). For (c) the upper inlet height of 1 m is compared to estimates of mixing height h_z from the MAR model (Gallée et al., 2014). Calculated flux values of NO_x were removed when $h_z < 10$ m resulting in the removal of 22 % (773 values) of all available 10 min flux averages. For (d) 10 min averages of $[c(z_2) - c(z_1)]$ not significantly different from zero, i.e. smaller than their respective 1-σ standard error, were not included in the calculation of the flux of NO_x. The 1-σ standard error in $[c(z_2) - c(z_1)]$ was determined by error propagation of the 1-σ standard error of NO_x mixing ratios. A total of 8 % (303 values) of all available 10 min flux averages were not significantly different from zero and thus removed.

In summary, the restrictions imposed by MOST and NO_x measurement uncertainty justify placing inlets at 0.01 and 1.0 m and lead to the removal of 30 % (1076 values) of all available flux estimates. The total uncertainty of the 10 min NO_x flux values due to random error in $[c(z_2) - c(z_1)]$ (31 %), u_* (3 % after Bauguitte et al., 2012) and measurement height (error in $\ln(z_2/z_1)$ of ~ 7 %) amounts to 32 %.

2.2 MAX-DOAS observations

Scattered sunlight was observed by a ground-based UV-visible spectrometer, in order to retrieve bromine oxide (BrO) column amounts. The instrument was contained in a small temperature-controlled box, which was mounted onto a tripod at 1 m above the snow surface. An external gearbox and motor scanned the box in elevation (so-called Multiple Axis). Spectra were analysed by Differential Optical Absorption Spectroscopy

ACPD
14, 31281–31317, 2014

(DOAS), the combination being known as the MAX-DOAS technique. See Roscoe et al. (2014) for more details of apparatus and analysis. Briefly, the observed spectrum contains Fraunhofer lines from the Sun's atmosphere, which interfere with absorption lines in the Earth's atmosphere and are removed by dividing by a reference spectrum. The amounts of absorbers in the Earth's atmosphere are found by fitting laboratory cross-sections to the ratio of observed to reference spectra, after applying a high-pass filter in wavelength (the DOAS technique).

In our case the spectral fit was from 341 to 356 nm, and the interfering gases O_3, O_4 (oxygen dimer) and NO_2 were included with BrO. The analysis was done with two reference spectra, one from near the start of the campaign in December, the other following the addition of a snow excluder in January, necessary because it also contained a blue glass filter with very different spectral shape. The analysis was restricted to cloud-free days or part-days. In MAX-DOAS geometry, the stratospheric light path is almost identical in low-elevation and zenith views, so stratospheric absorption is removed by subtracting simultaneous zenith amounts from low-elevation slant amounts, important for BrO as there is much in the stratosphere.

2.3 Ancillary measurements and data

Other co-located measurements included mixing ratios of OH radicals and the sum of peroxy radicals (RO_2) at 3 m using chemical ionisation mass spectrometry (Kukui et al., 2014) and mixing ratios of O_3 at 1 m with a UV absorption monitor (Thermo Electron Corporation model 49I, Franklin, Massachusetts). Standard meteorology was available from an automatic weather station (AWS) at 0.5 km distance and included air temperature (Vaisala PT100 DTS12 at 1.6 m), relative humidity at 1.6 m, wind speed and direction (Vaisala WAA 15A at 3.3 m). Photolysis rate coefficients, J, were determined based on actinic flux, I, measured at $\sim$ 3.50 m above the snow surface with a Met-Con 2π spectral radiometer equipped with a CCD detector and a spectral range from 285 to 700 nm (see also Kukui et al., 2014). During this study NO_3^- concentrations in snow were measured every 2–3 days in the surface skin layer, i.e. in the top 0.5 cm

ACPD
14, 31281–31317, 2014

of the snowpack, as well as in shallow snow pits within the clean-air sector. Snow NO_3^- concentrations were determined using clean sampling procedures and a continuous flow analysis technique (e.g. Frey et al., 2009b). Total column O_3 above Dome C was taken from ground based SAOZ (Système d'Analyse par Observation Zenitale) observations (http://saoz.obs.uvsq.fr/SAOZ_consol_v2.html). The mixing height h_z of the atmospheric boundary layer was calculated from simulations with the MAR model as the height where the turbulent kinetic energy decreases below 5 % of the value of the lowest layer of the model (Gallée et al., 2014).

2.4 Modelling NO_3^- photolysis

The flux of NO_2, F_{NO_2}, from the snowpack owing to photolysis of the NO_3^- anion in the snowpack can be estimated as the depth-integrated photolysis rate of NO_3^-

$$F_{NO_2} = \int_{z=0\,m}^{z=1\,m} [NO_3^-]_z \, J_z(NO_3^-) \, dz \quad (3)$$

where $J_z(NO_3^-)$ is the photolysis rate coefficient of reaction $NO_3^- + h\nu \rightarrow NO_2 + O^-$ at depth, z, in the snowpack. $[NO_3^-]_z$ is the amount of nitrate per unit volume of snow at depth, z, in the snowpack. $J(NO_3^-)$ is calculated as described in France et al. (2010) using a radiative transfer model, TUV-snow (Lee-Taylor and Madronich, 2002), to calculate irradiances within the snowpack as a function of depth. The optical properties and detailed description of the Dome C snowpack are reported in France et al. (2011). Values of depth-integrated flux were calculated as a function of solar zenith angle and scaled by values of $J(NO_3^-)$ measured by the Met-Con 2π spectral radiometer described above to account for changing sky conditions. Scaling by a measured value of $J(NO_3^-)$ is more accurate than previous efforts of scaling with a broad band UV instrument (e.g. France et al., 2011). The quantum yield and the absorption spectrum for nitrate photolysis in snow were taken from Chu and Anastasio (2003).

ACPD
14, 31281–31317, 2014

3 Results and discussion

3.1 NO_x observations in ambient and firn air

In summer 2011–2012 atmospheric mixing ratios of NO_x with strong diurnal variability were observed (Fig. 1c), similar to the 2009–2010 season, and showed maximum median levels in firn air of ~ 3837 pptv, which rapidly decreased to 319 pptv at 0.01 m and 213 pptv at 1.0 m (Table 1). As seen previously at Dome C and other locations, NO_x mixing ratios were weakly but significantly anti-correlated with wind speed (e.g. at 1.0 m $R^2 = 0.14$, $p < 0.001$) and their diurnal cycle was dampened during storms (Fig. 1b and c).

The two main differences between summer 2011–2012 and summer 2009–2010 are a strong intra-seasonal trend and larger atmospheric mixing ratios. A significant increase of NO_x mixing ratios at 1.0 m from low values in late November 2011 (Period I.) occurred in two steps: a small rise in the first week of December (Period II.), followed by a strong increase of daily averages from 300 to 1200 pptv during 9–11 December 2011 (Period III.) (Fig. 1c). After that NO_x mixing ratios gradually dropped over 10 days (Periods III.–IV.) to late November average concentrations of ~ 120 pptv (Fig. 1c). During 9–22 December 2011 (Period III.) the median concentration of NO_x at 1.0 m was 451 pptv, about 2.5 that during the same time period in 2009, but similar thereafter (Fig. 1c, Table 2).

The NO_x fluxes, F_{NO_x}, between 0.01 and 1.0 m were mostly emissions from the snow surface, with a median (range) of 1.6 (0.4–2.9) $\times 10^{13}$ molecule m^{-2} s^{-1} and showed an increase by a factor 3, approximately around the same time when atmospheric mixing ratios of NO_x increased (Period III.) (Fig. 1d, Table 1). The median flux of NO_x during 9–22 December 2011 reached 3.1 $\times 10^{13}$ molecule m^{-2} s^{-1}, about 5 times the season median from 2009–2010. During 23 December to 12 January (Period IV.) the median flux of NO_x in 2011–2012 was about twice that observed in 2009–2010 (Table 2). Po-

ACPD
14, 31281–31317, 2014

tential causes of significant variability in mixing ratios and flux on seasonal time scales are discussed in Sect. 3.5.

3.2 The lower atmosphere-firn air profile

On 9 January 2012 a total of 12 vertical atmospheric profiles of NO_x mixing ratios were measured between 11:30 and 23:30 LT. The lower 100 m of the atmosphere appear well mixed throughout the afternoon, with mixing heights h_z of 200–550 m and observed turbulent diffusion coefficients of heat K_h of $\sim 0.1\,m^2\,s^{-1}$ (Fig. 2). However, in the late afternoon K_h values decreased gradually over a few hours to reach in the evening levels half those during the day thereby giving evidence of strongly reduced vertical mixing. Furthermore, around 18:30 LT h_z values decreased within minutes from 550 to < 15 m height (Fig. 2a) illustrating the collapse of the convective boundary layer typically observed at Dome C in the early evening during summer (King et al., 2006). It follows that NO_x snow emissions are trapped near the surface and caused a significant increase in NO_x mixing ratios below 15 m height measured almost immediately after collapse of the boundary layer (Fig. 2). During 22:20–22:40 LT a small increase in K_h, due to the nightly increase in wind shear (see Frey et al., 2013), was sufficient to cause upward mixing of NO_x accumulated near the surface to ~ 35 m height (Fig. 2). The vertical balloon soundings further underline the unique geographical setting of Dome C or other sites of similar latitude on the East Antarctic Plateau where air chemistry is dominated by strong diurnal cycles, both in down-welling solar radiation and atmospheric stability, contrasting South Pole where diurnal changes are absent and changes are more due to synoptic variability (Neff et al., 2008).

A vertical profile of mixing ratios of NO_x and O_3 in firn air was measured on 12 January 2012 between 10:00 and 18:00 LT, for which depths were sampled in random order for 30–60 min each. Mixing ratio maxima of NO and NO_2 were ~ 1 and 4 ppbv, respectively, about one order of magnitude above ambient air levels (Table 1), and occurred at 10–15 cm depth, slightly below the typical e-folding depth of 10 cm of wind pack snow at Dome C (France et al., 2011) (Fig. 3a). NO dropped off quickly with

ACPD
14, 31281–31317, 2014

depth, reaching 55 pptv at 85 cm, whereas NO_2 decreased asymptotically approaching ~ 2 ppbv (Fig. 3a). NO_3^- concentrations in snow under the firn air probe did not follow the exponential decrease with depth typically observed at Dome C (e.g. Erbland et al., 2013), but values within one e-folding depth were still in the range measured further away (Profiles P1–P3 in Fig. 3a), justifying a discussion of vertical trends. O_3 mixing ratios in firn air were always below ambient air levels, suggesting the snow pack to be an O_3 sink as observed previously for the snowpack on the Greenland ice sheet (Peterson and Honrath, 2001), and showed a significant anti-correlation with NO_2 (R^2 = 0.7, $p < 0.001$). This is further evidence for significant release of NO_x by the snow matrix into the interstitial air, which then titrates O_3 through the reaction $NO + O_3 \rightarrow NO_2 + O_2$ (Fig. 3). In particular, the elevated NO_2 concentration at 45 cm was not an outlier, as indicated by the collocated drop of O_3 by > 10 ppbv compared to adjacent snow layers, but was possibly due to snow with large NO_3^- concentrations (Fig. 3a). The observed vertical trends in NO_x suggest that below a few e-folding depths the open pore space of the upper snowpack holds a significant reservoir of NO_2 produced photolytically above, as hypothesized previously (Frey et al., 2013). In contrast, NO disappears at depths devoid of UV irradiance as it reacts with O_3.

3.3 Response to UV irradiance

Changes in surface downwelling UV irradiance lead to a quick response of mixing ratios and speciation of NO_x in ambient and firn air as observed during a partial solar eclipse and during a shading experiment (Fig. 4). The solar eclipse occurred early in the season, on 25 November 2011, and caused a decrease in ambient NO mixing ratios at 1.0 m by about 10 pptv or 10 %, whereas NO_2 mixing ratios did not change significantly (Fig. 4a and b). The NO gas phase source, UV photolysis of NO_2, is reduced during the solar eclipse. But the sink of NO, the fast titration with O_3, is unaffected by the reduction in UV irradiance. During the shading experiment on 11 January 2012 plastic sheets were placed at 1 m above the snow surface, alternating in 30 min intervals between UV-opaque and UV-transparent materials. The impact of blocking incident UV irradiance

ACPD
14, 31281–31317, 2014

(wavelengths < 380 nm) on firn air mixing ratios at 10 cm snow depth was up to 300 pptv or 30 % decrease in mixing ratios of NO, whereas mixing ratios of NO_2 increased at the same time by ∼ 150 pptv or 5 %, although often not statistically significant (Fig. 4c and d). Similar to the solar eclipse, the behavior of NO_x mixing ratios in firn air is in accordance with a disruption of the fast gas phase interconversion of NO_x species. Decrease of NO and increase of NO_2 mixing ratios are consistent with the suppression of NO_2 photolysis, which is both a NO source and a NO_2 sink.

Most importantly varying incident UV irradiance in the wavelength region of NO_3^- absorption (action spectrum maximum at 320 nm) over half-hourly time scales does not cause a depletion of NO_2 in firn air even though NO_2 is the main product of NO_3^- photolysis in the snowpack. A dampened UV response of NO_2 mixing ratios suggests that the NO_x reservoir present in the open pore space of the upper snow pack discussed above must be large as it is not depleted during 30 min filter changes at the sample pump rates used. One implication is that the impact of changes in incident UV irradiance on the snow source and thus NO_x flux and mixing ratios is only observable on diurnal and seasonal time scales.

3.4 NO_2 : NO ratios, peroxy and halogen radicals

In 2011–2012 the NO_2 : NO ratios at 1.0 m were up to 3 times larger than in 2009–2010 (Table 2). A previous steady-state analysis indicated that high peroxy and possibly halogen radical levels must be present to explain large deviations from the simple Leighton steady-state (Frey et al., 2013). During summer 2011–2012 median concentrations of RO_2 radicals at 3 m were 9.9×10^7 molecule cm^{-3} (Kukui et al., 2014). To find the vertical amounts of BrO radicals the MAX-DOAS measurements were evaluated as follows: we divided by the ratio of the slant path length to the vertical (the Air Mass Factor, AMF), calculated by radiative transfer code (Mayer and Kylling, 2005), assuming all the BrO was in the lowest 200 m. Figure 5 shows the BrO results, where the apparent vertical amounts at 15° are much larger than those at lower elevations – the AMFs are incorrect, and interestingly, as at Halley in 2007 (Roscoe et al., 2014), much of the BrO

ACPD
14, 31281–31317, 2014

must be in the free troposphere. The average of BrO at the three elevations is about 0.8 $\times 10^{13}$ molecule cm^{-2}, with a slight decrease during the campaign. The average at Halley in 2007 was about 2.5 $\times 10^{13}$ molecule cm^{-2}, so mixing ratios of BrO at Dome C are about a third those at Halley. The Dome C data were not inverted to determine the mixing ratio near the surface, but the changes in slant column with elevation angle are similar to those at Halley in 2007 (Roscoe et al., 2014). So if the Halley inversion results are simply divided by 3 the Dome C values imply 2 to 3 pptv of BrO near the surface.

The same steady-state calculation as described by Frey et al. (2013) was repeated for austral summer 2011–2012 and yields an average of 2.6×10^9 molecule cm^{-3} or 134 pptv of total radical concentrations [OX] = [HO_2]+[RO_2]+2[XO] (Ridley et al., 2000). The steady-state estimates of RO_2 radicals are therefore $\sim$ 20 times those observed at mid day by Kukui et al. (2014). While observed BrO and RO_2 radicals are too low to explain the large NO_2 : NO ratios it is possible that at least part of this inconsistency may be due to overestimated NO_2 from a potential interference with HNO_4 (not measured) as discussed above.

3.5 Drivers of seasonal NO_x variability

On diurnal time scales NO_x mixing ratios at Dome C are controlled by the interplay between snow pack source strength and atmospheric physical properties, i.e. turbulent diffusion coefficient of heat K_h and mixing height h_z of the boundary layer (Frey et al., 2013). Indeed, median diurnal cycles of NO_x mixing ratios during 1–8 December 2011 (Period II.) showed previously described behavior (Frey et al., 2013) with a strong maximum during 18:00–20:00 LT and a minimum at 01:00 LT, then during 9–22 December 2011 (Period III.) at similar noon time values further increase of the primary maximum and generally large mixing ratios during night time (Fig. 6a). During 23 December 2011–2012 January 2012 (Period IV.) the diurnal cycle of NO_x mixing ratios returned to low values and small diurnal amplitudes (Fig. 6a). As expected the NO_x emission flux F_{NO_x} between 0.01 and 1.0 m always peaked at local noon, but showed

ACPD
14, 31281–31317, 2014

during 9–22 December 2011 (Period III.) a strong increase at all times of the day with a near doubling of the noon time median (Fig. 6b). Below we evaluate potential causes of the unusual variability in NO_x mixing ratios and flux observed on seasonal time scales.

3.5.1 Atmospheric mixing vs. snow source strength

Similar to explaining diurnal NO_x cycles at Dome C the seasonal trends of daily mean NO_x mixing ratios during the first half of December 2011 can be attributed to a combination of changes in F_{NO_x} and h_z (Fig. 1). The strong increase of NO_x around 11 December 2011 falls into a period when F_{NO_x} almost tripled, but shallow boundary layer depths prevailed with daily h_z maxima below 100–200 m (Fig. 1). After 12 December 2011 F_{NO_x} remained at high values, thus, the decrease of NO_x mixing ratios appears to be primarily caused by daily maximum h_z increasing to > 600 m on 18 December 2011 (Fig. 1). After 23 December NO_x mixing ratios drop to low levels, due to smaller F_{NO_x} and a deep boundary layer (Fig. 1).

Trends in F_{NO_x} are controlled by variability in atmospheric turbulence (K_h) and concentration differences (ΔNO_x), which in turn are determined by the strength of the photolytic snow pack source (Eq. 2). However, the relative importance of K_h and snow pack source strength can vary. For example, during 23 December 2011–12 January 2012 (Period IV.) the median F_{NO_x} was 1.3×10^{13} molecule $m^{-2}\,s^{-1}$, about twice that observed during the same period in 2009–2010 (Fig. 6g; Table 2). The inter-seasonal difference can be explained by both, significantly larger atmospheric turbulence and more negative ΔNO_x during all times of the day in 2011–2012 (Fig. 6h and i). Median K_h was 0.08 $m^2\,s^{-1}$, double that in 2009–2010, and median ΔNO_x was −51 pptv compared to −32 pptv in 2009–2010 (Table 2). In contrast, during 2011–2012 the observed intra-seasonal variability of F_{NO_x} is dominated by changes in the snow pack source strength. During 9–22 December 2011 (Period III.) median K_h values ($\sim 0.05\,m^2\,s^{-1}$) and diurnal cycles were smaller than thereafter (Fig. 6c; Table 2), while ΔNO_x values

ACPD
14, 31281–31317, 2014

were among the largest observed so far at Dome C, about three times those during the rest of the season, and therefore primarily caused the tripling of F_{NO_x} (Fig. 6d and i).

3.5.2 Snow source strength

A number of factors may contribute to changes in snow source strength of NO_x. One possibility to explain increases in F_{NO_x} is that the NO_2 reservoir in the open pore space of the upper snowpack discussed above may undergo venting upon changes in atmospheric pressure. However, no statistically significant relationship between F_{NO_x} and atmospheric pressure is found (data not shown). The main cause of large F_{NO_x} values appears rather to be related to changes in snow production rates of NO_x from NO_3^- photolysis, which depend on the NO_3^- photolysis rate coefficient $J_{NO_3^-}$ and the NO_3^- concentration in the photic zone of the snow pack (Eq. 3).

Trends in down-welling UV irradiance due to stratospheric O_3 depletion were suggested previously to drive $J_{NO_3^-}$ and therefore F_{NO_x} and the associated increase in net production of surface O_3 at South Pole (Jones and Wolff, 2003). At Dome C the observed increase in F_{NO_x} and strongly negative ΔNO_x values coincided with a period when total column O_3 declined from > 300 to about 250 DU (Fig. 7a and c). During 9–22 December 2011 (Period III.) the median column O_3 was about 8 % lower than during the time periods before and after (Table 2). However, associated changes in $J_{NO_3^-}$ on the order of ∼ 10 % are too small to account alone for the observed tripling in F_{NO_x} (Fig. 6e; Table 2).

Instead changes in F_{NO_x} can be linked to the temporal variability of NO_3^- present in the snow skin layer. During time periods II. and III. skin layer NO_3^- concentrations were up to two times larger than before and after, coinciding with increased F_{NO_x} (Fig. 7b and c). To confirm this F_{NO_2} values were modelled based on observed $J_{NO_3^-}$, daily sampling of skin layer NO_3^- and two depth profiles, at 100 m (P1) and 5 km (P2) distance from the lab shelter, in order to account for spatial and temporal variability in NO_3^-

ACPD
14, 31281–31317, 2014

concentrations of surface snow. Modelled F_{NO_2} capture some of the temporal trends in observational estimates of F_{NO_x} confirming the link with $J_{NO_3^-}$ and NO_3^- concentrations (Fig. 7c). However, median ratios of observed F_{NO_x} and modelled F_{NO_2} values are 30–50 during Period III. and 15–30 during Period IV. (Fig. 7c).

Disagreement between model and observations was previously attributed to uncertainties in the quantum yield of NO_3^- photolysis in natural snow (Frey et al., 2013). The model employed here uses a constant quantum yield, i.e. its value at the mean ambient temperature at Dome C (−30 °C) of 0.0019 (Chu and Anastasio, 2003). The same lab study reports a positive relationship between quantum yield and temperature (Chu and Anastasio, 2003). Comparison of time periods before and after 18 December 2011 shows an increase of mean air temperature from −34.2 °C to −27.7 °C and a decrease of its mean diurnal amplitude from 13 to 9.7 K (Fig. 1a). However, observations of F_{NO_x} showed behaviour opposite to that expected from a temperature driven quantum yield, i.e. F_{NO_x} values decreased as air temperature increased (Fig. 1a and d). Yet, the large diurnal amplitude of air temperature at Dome C could explain diurnal changes of F_{NO_x} by a factor 1.5–1.75. The temperature effect is however small when compared to the observed 20-fold change between night and day in F_{NO_x}, which are driven by actinic flux. A recent lab study found that the quantum yield of photolytic loss of nitrate from snow samples collected at Dome C decreased from 0.44 to 0.003 within what corresponds to days of UV exposure in Antarctica (Meusinger et al., 2014). The authors argue that the observed decrease in quantum is due to nitrate being made of a photo-labile and a photo-stabile fraction, confirming a previous hypothesis that the range of quantum yields reflects the location of NO_3^- within the snow grain and therefore availability to photolysis (Frey et al., 2013). Thus, observed F_{NO_x} values fall well within the range of predictions based on quantum yield values measured in Dome C snow, which exceed that used in the current model by a factor 2–200. A systematic decrease in quantum yield due to depletion of photo-labile NO_3^- in surface snow may have contributed to the observed decrease in F_{NO_x} after 22 December 2011. However, a lack of information on snow grain morphology or NO_3^- location within the snow grain limits

ACPD
14, 31281–31317, 2014

further exploration of the impact of a time variable quantum yield on F_{NO_x}. It should be noted that during 2009–2010 large skin layer NO_3^- values did not result in F_{NO_x} values comparable to those in 2011–2012 which may be due to a different partitioning between photolabile and photostabile NO_3^- in surface snow (Fig. 7b and c; Table 2).

The consequences of large NO_x fluxes consist not only in contributing to high NO_x mixing ratios but also in influencing local O_3 production, as suggested by significantly higher surface O_3 mixing ratios (> 30 ppbv) during 9–22 December in 2011–2012 (Period III.) than in 2009–2010 (Fig. 7d).

4 Conclusions

Measurements of NO_x mixing ratios and flux carried out as part of the OPALE campaign at Dome C in 2011–2012 allowed to extend the existing data set from a previous campaign in 2009–2010.

Vertical profiles of the lower 100 m of the atmosphere confirm that at Dome C strong diurnal cycles, both in down-welling solar radiation and atmospheric stability, control the variability of NO_x mixing ratios and flux. In contrast, at South Pole diurnal cycles are absent and changes more due to synoptic variability (Neff et al., 2008). Understanding atmospheric composition and air-snow interactions in inner Antarctica requires studies at both sites as they together encompass the spectrum of diurnal variability expected across the East Antarctic Plateau (King et al., 2006; Frey et al., 2013).

Firn air profiles suggest that the upper snow pack at Dome C is a O_3 sink and holds below a few e-folding depths a significant reservoir of NO_2 produced photolytically above, whereas NO disappears at depths devoid of UV as it reacts with O_3. Shading experiments showed that the presence of such a NO_2 reservoir dampens the response of NO_x mixing ratios above or within the snowpack due to changes in down-welling UV irradiance on hourly time scales. Thus, systematic changes in NO_x mixing ratios and flux due to the impact of UV on the snow source are only observable on diurnal and seasonal time scales.

ACPD
14, 31281–31317, 2014

First-time observations of BrO at Dome C suggest 2–3 pptv near the ground, with higher levels in the free troposphere similar to Halley, possibly originating from a sea ice source in coastal Antarctica (Theys et al., 2011) or from stratospheric descent (Salawitch et al., 2010). Assuming steady-state observed mixing ratios of BrO and RO_2 radicals are too low to explain the large NO_2 : NO ratios found in ambient air. It is possible that HNO_4, likely present at Dome C but not measured during OPALE, may cause an overestimate of NO_2 with the detection method employed and may therefore explain part of this inconsistency.

During 2011–2012 NO_x mixing ratios and flux were larger than in 2009–2010 consistent with also larger surface O_3 mixing ratios resulting from increased net O_3 production. Large NO_x mixing ratios and significant variability during December 2011 were attributed to a combination of changes in mixing height and NO_x snow emission flux F_{NO_x}. Trends in F_{NO_x} were found to be controlled by atmospheric turbulence and the strength of the photolytic snowpack source, of which the relative importance may vary in time. Larger median F_{NO_x} values in 2011–2012 than those during the same period in 2009–2010 can be explained by both, significantly larger atmospheric turbulence and a slightly stronger snowpack source. However, the tripling of F_{NO_x} in December 2011 was largely due to changes in snow pack source strength driven primarily by changes in NO_3^- concentrations in the snow skin layer, and only to a secondary order by decrease of total column O_3 and associated increase in NO_3^- photolysis rates. Median ratios of observed F_{NO_x} and modelled F_{NO_2} values ranged from 15 to 50 using the quantum yield of NO_3^- photolysis reported by Chu and Anastasio (2003). Model predictions based on quantum yield values measured in a recent lab study on Dome C snow samples (Meusinger et al., 2014) yield 2–200 fold larger F_{NO_2} values encompassing observed F_{NO_x}. In particular, a decrease in quantum yield due to depletion of photo-labile NO_3^- in surface snow may have contributed to the observed decrease in F_{NO_x} after 22 December 2011. Yet in 2009–2010 large skin layer NO_3^- values did not result in elevated F_{NO_x} values as seen in 2011–2012 possibly due to different partitioning of NO_3^- between a photo-labile and photo-stabile fraction. In summary the seasonal variability

ACPD
14, 31281–31317, 2014

of NO_x snow emissions important to understand atmospheric composition above the East Antarctic Plateau depends not only on atmospheric mixing but also critically on snow NO_3^- concentrations and incident UV irradiance. Future studies need to address how quantum yield of NO_3^- photolysis varies in time as a function of snow chemical and physical properties thereby obtaining a more detailed view on the dynamics in the vertical redistribution of NO_3^- across the sunlit snowpack driven by photolysis and redeposition (e.g. Frey et al., 2009b).

Acknowledgements. M. M. Frey is funded by the Natural Environment Research Council through the British Antarctic Survey Polar Science for Planet Earth Programme. This study was supported by core funding from NERC to BAS's Chemistry & Past Climate Program. The OPALE project was funded by the ANR (Agence National de Recherche) contract ANR-09-BLAN-0226. National financial support and field logistic supplies for the summer campaign were provided by Institut Polaire Français-Paul Emile Victor (IPEV) within programs No. 414, 903, and 1011. J. L. France and M. D. King wish to thank NERC NE/F0004796/1 and NE/F010788, NERC FSF 20 grants 555.0608 and 584.0609. We thank B. Jourdain for assistance with balloon soundings and firn air experiments, PNRA for meteorological data and IPEV for logistic support. We are also grateful to J. Dibb and D. Perovich for valuable input on the design of the firn air probe. Collected data are accessible through NERC's Polar Data Centre.

References

Anderson, P. S. and Neff, W. D.: Boundary layer physics over snow and ice, Atmos. Chem. Phys., 8, 3563–3582, doi:10.5194/acp-8-3563-2008, 2008. 31289

Bauguitte, S. J.-B., Bloss, W. J., Evans, M. J., Salmon, R. A., Anderson, P. S., Jones, A. E., Lee, J. D., Saiz-Lopez, A., Roscoe, H. K., Wolff, E. W., and Plane, J. M. C.: Summertime NO_x measurements during the CHABLIS campaign: can source and sink estimates unravel observed diurnal cycles?, Atmos. Chem. Phys., 12, 989–1002, doi:10.5194/acp-12-989-2012, 2012. 31284, 31290

Chu, L. and Anastasio, C.: Quantum yields of hydroxyl radical and nitrogen dioxide from the photolysis of nitrate on ice, J. Phys. Chem. A, 107, 9594–9602, 2003. 31292, 31300, 31302

ACPD
14, 31281–31317, 2014

Cohen, L., Helmig, D., Neff, W. D., Grachev, A. A., and Fairall, C. W.: Boundary-layer dynamics and its influence on atmospheric chemistry at Summit, Greenland, Atmos. Environ., 41, 5044–5060, doi:10.1016/j.atmosenv.2006.06.068, 2007. 31284

Crawford, J. H., Davis, D. D., Chen, G., Buhr, M., Oltmans, S., Weller, R., Mauldin, L., Eisele, F., Shetter, R., Lefer, B., Arimoto, R., and Hogan, A.: Evidence for photochemical production of ozone at the South Pole surface, Geophys. Res. Lett., 28, 3641–3644, 2001. 31285

Davis, D. D., Seelig, J., Huey, G., Crawford, J., Chen, G., Wang, Y. H., Buhr, M., Helmig, D., Neff, W., Blake, D., Arimoto, R., and Eisele, F.: A reassessment of Antarctic plateau reactive nitrogen based on ANTCI 2003 airborne and ground based measurements, Atmos. Environ., 42, 2831–2848, doi:10.1016/j.atmosenv.2007.07.039, 2008. 31284, 31285

Erbland, J., Vicars, W. C., Savarino, J., Morin, S., Frey, M. M., Frosini, D., Vince, E., and Martins, J. M. F.: Air–snow transfer of nitrate on the East Antarctic Plateau – Part 1: Isotopic evidence for a photolytically driven dynamic equilibrium in summer, Atmos. Chem. Phys., 13, 6403–6419, doi:10.5194/acp-13-6403-2013, 2013. 31295

Fisher, F. N., King, M. D., and Lee-Taylor, J.: Extinction of UV-visible radiation in wet mid-latitude (maritime) snow: Implications for increased NO_x emission, J. Geophys. Res., 110, doi:10.1029/2005JD005963, 2005. 31284

France, J. L., King, M. D., and Lee-Taylor, J.: The importance of considering depth-resolved photochemistry in snow: a radiative-transfer study of NO_2 and OH production in Ny-Alesund (Svalbard) snowpacks, J. Glaciol., 56, 655–663, 2010. 31292

France, J. L., King, M. D., Frey, M. M., Erbland, J., Picard, G., Preunkert, S., MacArthur, A., and Savarino, J.: Snow optical properties at Dome C (Concordia), Antarctica; implications for snow emissions and snow chemistry of reactive nitrogen, Atmos. Chem. Phys., 11, 9787–9801, doi:10.5194/acp-11-9787-2011, 2011. 31292, 31294

Frey, M. M., Stewart, R. W., McConnell, J. R., and Bales, R. C.: Atmospheric hydroperoxides in West Antarctica: links to stratospheric ozone and atmospheric oxidation capacity, J. Geophys. Res., 110, D23301, doi:10.1029/2005JD006110, 2005. 31285

Frey, M. M., Hutterli, M. A., Chen, G., Sjostedt, S. J., Burkhart, J. F., Friel, D. K., and Bales, R. C.: Contrasting atmospheric boundary layer chemistry of methylhydroperoxide (CH_3OOH) and hydrogen peroxide (H_2O_2) above polar snow, Atmos. Chem. Phys., 9, 3261–3276, doi:10.5194/acp-9-3261-2009, 2009. 31285

Frey, M. M., Savarino, J., Morin, S., Erbland, J., and Martins, J. M. F.: Photolysis imprint in the nitrate stable isotope signal in snow and atmosphere of East Antarctica and implications for

ACPD
14, 31281–31317, 2014

reactive nitrogen cycling, Atmos. Chem. Phys., 9, 8681–8696, doi:10.5194/acp-9-8681-2009, 2009b. 31284, 31292, 31303

Frey, M. M., Brough, N., France, J. L., Anderson, P. S., Traulle, O., King, M. D., Jones, A. E., Wolff, E. W., and Savarino, J.: The diurnal variability of atmospheric nitrogen oxides (NO and NO_2) above the Antarctic Plateau driven by atmospheric stability and snow emissions, Atmos. Chem. Phys., 13, 3045–3062, doi:10.5194/acp-13-3045-2013, 2013. 31284, 31285, 31286, 31287, 31288, 31289, 31290, 31294, 31295, 31296, 31297, 31300, 31301, 31310, 31317

Gallée, H., Preunkert, S., Jourdain, B., Argentini, S., Frey, M. M., Genthon, C., Legrand, M., Pietroni, I., and Casasanta, G.: Characterization of the boundary layer at Dome C during OPALE, Atmos. Chem. Phys. Discuss., in press, 2014. 31290, 31292, 31311

Honrath, R. E., Peterson, M. C., Dziobak, M. P., Dibb, J., Arsenault, M. A., and Green, S. A.: Release of NO_x from sunlight-irradiated midlatitude snow, Geophys. Res. Lett., 27, 2237–2240, 2000a. 31284

Honrath, R. E., Guo, S., Peterson, M. C., Dziobak, M. P., Dibb, J. E., and Arsenault, M. A.: Photochemical production of gas phase NO_x from ice crystal NO_3^-, J. Geophys. Res., 105, 24183–24190, 2000b. 31284

Honrath, R., Lu, Y., Peterson, M., Dibb, J., Arsenault, M., Cullen, N., and Steffen, K.: Vertical fluxes of NO_x, HONO, and HNO_3 above the snowpack at Summit, Greenland, Atmos. Environ., 36, 2629–2640, doi:10.1016/S1352-2310(02)00132-2, 2002.

Jacobson, M. Z.: Fundamentals of Atmospheric Modeling, Cambridge University Press, Cambridge, UK, 1999. 31288, 31289

Jones, A. E. and Wolff, E. W.: An analysis of the oxidation potential of the South Pole boundary layer and the influence of stratospheric ozone depletion, J. Geophys. Res., 108, doi:10.1029/2003JD003379, 2003. 31299

Jones, A. E., Weller, R., Anderson, P. S., Jacobi, H. W., Wolff, E. W., Schrems, O., and Miller, H.: Measurements of NO_x emissions from the Antarctic snow pack, Geophys. Res. Lett., 28, 1499–1502, 2001. 31284

Kaimal, J. and Finnigan, J. J.: Atmospheric Boundary Layer Flows, Oxford University Press, Oxford, UK, 1994. 31289

King, J. C., Argentini, S. A., and Anderson, P. S.: Contrasts between the summertime surface energy balance and boundary layer structure at Dome C and Halley stations, Antarctica, J. Geophys. Res., 111, D02105, doi:10.1029/2005JD006130, 2006. 31294, 31301

ACPD
14, 31281–31317, 2014

Kukui, A., Legrand, M., Preunkert, S., Frey, M. M., Loisil, R., Gil Roca, J., Jourdain, B., King, M. D., France, J. L., and Ancellet, G.: Measurements of OH and RO_2 radicals at Dome C, East Antarctica, Atmos. Chem. Phys., 14, 12373–12392, doi:10.5194/acp-14-12373-2014, 2014. 31291, 31296, 31297

Lee-Taylor, J. and Madronich, S.: Calculation of actinic fluxes with a coupled atmosphere-snow radiative transfer model, J. Geophys. Res., 107, 4796, doi:10.1029/2002JD002084, 2002. 31292

Legrand, M., Preunkert, S., Jourdain, B., Gallée, H., Goutail, F., Weller, R., and Savarino, J.: Year-round record of surface ozone at coastal (Dumont d'Urville) and inland (Concordia) sites in East Antarctica, J. Geophys. Res., 114, D20306, doi:10.1029/2008JD011667, 2009. 31285

Legrand, M., Preunkert, S., Frey, M., Bartels-Rausch, Th., Kukui, A., King, M. D., Savarino, J., Kerbrat, M., and Jourdain, B.: Large mixing ratios of atmospheric nitrous acid (HONO) at Concordia (East Antarctic Plateau) in summer: a strong source from surface snow?, Atmos. Chem. Phys., 14, 9963–9976, doi:10.5194/acp-14-9963-2014, 2014. 31287, 31288

Lenschow, D. H.: Micrometeorological techniques for measuring biosphere–atmosphere trace gas exchange, in: Biogenic Trace Gases: Measuring Emissions from Soil and Water, edited by: Matson, P. A. and Harriss, R. C., Blackwell Science, London, 126–163, 1995. 31289

Mayer, B. and Kylling, A.: Technical note: The libRadtran software package for radiative transfer calculations – description and examples of use, Atmos. Chem. Phys., 5, 1855–1877, doi:10.5194/acp-5-1855-2005, 2005. 31296

Meusinger, C., Berhanu, T. A., Erbland, J., Savarino, J., and Johnson, M. S.: Laboratory study of nitrate photolysis in Antarctic snow. I. Observed quantum yield, domain of photolysis, and secondary chemistry, J. Chem. Phys., 140, 244305, doi:10.1063/1.4882898, 2014. 31285, 31300, 31302

Neff, W., Helmig, D., Grachev, A., and Davis, D.: A study of boundary layer behavior associated with high NO concentrations at the South Pole using a minisodar, tethered balloons and sonic anemometer, Atmos. Environ., 42, 2762–2779, doi:10.1016/j.atmosenv.2007.01.033, 2008. 31284, 31294, 31301

Peterson, M. C. and Honrath, R. E.: Observations of rapid photochemical destruction of ozone in snowpack interstitial air, Geophys. Res. Lett., 28, 511–514, 2001. 31295

Preunkert, S., Ancellet, G., Legrand, M., Kukui, A., Kerbrat, M., Sarda-Estève, R., Gros, V., and Jourdain, B.: Oxidant Production over Antarctic Land and its Export (OPALE)

ACPD
14, 31281–31317, 2014

project: an overview of the 2010–2011 summer campaign, J. Geophys. Res., 117, doi:10.1029/2011JD017145, 2012. 31286

Ridley, B., Walega, J., Montzka, D., Grahek, F., Atlas, E., Flocke, F., Stroud, V., Deary, J., Gallant, A., Boudries, H., Bottenheim, J., Anlauf, K., Worthy, D., Sumner, A., Splawn, B., and Shepson, P.: Is the Arctic surface layer a source and sink of NO_x in winter/spring?, J. Atmos. Chem., 36, 1–22, doi:10.1023/A:1006301029874, 2000. 31297

Roscoe, H., Brough, N., Jones, A., Wittrock, F., Richter, A., Roozendael, M. V., and Hendrick, F.: Characterisation of vertical BrO distribution during events of enhanced tropospheric BrO in Antarctica, from combined remote and in-situ measurements, J. Quant. Spectrosc. Rad. Trans., 138, 70–81, doi:10.1016/j.jqsrt.2014.01.026, 2014. 31291, 31296, 31297

Salawitch, R. J., Canty, T., Kurosu, T., Chance, K., Liang, Q., da Silva, A., Pawson, S., Nielsen, J. E., Rodriguez, J. M., Bhartia, P. K., Liu, X., Huey, L. G., Liao, J., Stickel, R. E., Tanner, D. J., Dibb, J. E., Simpson, W. R., Donohoue, D., Weinheimer, A., Flocke, F., Knapp, D., Montzka, D., Neuman, J. A., Nowak, J. B., Ryerson, T. B., Oltmans, S., Blake, D. R., Atlas, E. L., Kinnison, D. E., Tilmes, S., Pan, L. L., Hendrick, F., Van Roozendael, M., Kreher, K., Johnston, P. V., Gao, R. S., Johnson, B., Bui, T. P., Chen, G., Pierce, R. B., Crawford, J. H., and Jacob, D. J.: A new interpretation of total column BrO during Arctic spring, Geophys. Res. Lett., 37, doi:10.1029/2010GL043798, 2010. 31302

Simpson, W. R., King, M. D., Beine, H. J., Honrath, R. E., and Zhou, X.: Radiation-transfer modeling of snow-pack photochemical processes during ALERT 2000, Atmos. Environ., 36, 2663–2670, 2002. 31284

Slusher, D. L., Neff, W. D., Kim, S., Huey, L. G., Wang, Y., Zeng, T., Tanner, D. J., Blake, D. R., Beyersdorf, A., Lefer, B. L., Crawford, J. H., Eisele, F. L., Mauldin, R. L., Kosciuch, E., Buhr, M. P., Wallace, H. W., and Davis, D. D.: Atmospheric chemistry results from the ANTCI 2005 Antarctic plateau airborne study, J. Geophys. Res., 115, D07304, doi:10.1029/2009JD012605, 2010. 31284, 31285, 31288

Stull, R. B.: An Introduction to Boundary Layer Meteorology, Kluwer Academic Publishers, Dordbrecht/Boston/London, 1988. 31290

Theys, N., Van Roozendael, M., Hendrick, F., Yang, X., De Smedt, I., Richter, A., Begoin, M., Errera, Q., Johnston, P. V., Kreher, K., and De Mazière, M.: Global observations of tropospheric BrO columns using GOME-2 satellite data, Atmos. Chem. Phys., 11, 1791–1811, doi:10.5194/acp-11-1791-2011, 2011. 31302

ACPD
14, 31281–31317, 2014

Van Dijk, A., Moen, A., and De Bruin, H.: The principles of surface flux physics: theory, practice and description of the ECPACK library, Internal Report 2004/1, Meteorology and Air Quality Group, Wageningen University, Wageningen, the Netherlands, 2006. 31289

Zatko, M. C., Grenfell, T. C., Alexander, B., Doherty, S. J., Thomas, J. L., and Yang, X.: The influence of snow grain size and impurities on the vertical profiles of actinic flux and associated NO_x emissions on the Antarctic and Greenland ice sheets, Atmos. Chem. Phys., 13, 3547–3567, doi:10.5194/acp-13-3547-2013, 2013. 31285

ACPD
14, 31281–31317, 2014

Table 1. NO_x mixing ratios and flux at Dome C during 23 November 2011–12 January 2012.

Parameter	z, m	mean $\pm 1\sigma$	median	t_{total}, days[a]
NO, pptv	−0.1[b]	1097 ± 795	879	2.9
	0.01	121 ± 102	94	18.6
	1.0	98 ± 80	77	24.4
	4.0	93 ± 68	78	13.7
NO_2, pptv	−0.1[b]	4145 ± 2667	2990	2.6
	0.01	328 ± 340	222	17.6
	1.0	211 ± 247	137	23.2
	4.0	210 ± 199	159	12.8
NO_x, pptv	−0.1[b]	5144 ± 3271	3837	2.6
	0.01	447 ± 432	319	17.5
	1.0	306 ± 316	213	23.2
	4.0	302 ± 259	241	12.8
$F-NO_x$ $\times 10^{13}$ molecule m^{-2} s^{-1}[c]	0.01–1.0	2.5 ± 8.2	1.6	17.4
$F-NO_x$ $\times 10^{13}$ molecule m^{-2} s^{-1}, local noon	0.01–1.0	5.0 ± 8.2	2.9	1.1
$F-NO_x$ $\times 10^{13}$ molecule m^{-2} s^{-1}, local midnight	0.01–1.0	0.3 ± 1.6	0.4	0.2

[a] Total sample time estimated as the sum of all 1 min intervals.
[b] Firn air sampled during 20–22 December 2011, 1–5 January 2012 and 10–14 January 2012.
[c] 1 December 2011–12 January 2012.

ACPD
14, 31281–31317, 2014

Table 2. Seasonal evolution of median NO_x mixing ratios and flux along with relevant environmental parameters at Dome C in summer 2011–2012 (time periods I.–IV. highlighted in Fig. 1 and 7) and comparison to summer 2009–2010 (from Frey et al., 2013).

Parameter	I. 23 Nov 2011–30 Nov 2011	II. 1 Dec 2011–8 Dec 2011	III. 9 Dec 2011–22 Dec 2011	IV. 23 Dec 2011–12 Jan 2012	9 Dec 2009–22 Dec 2009	23 Dec 2009–12 Jan 2010
NO_x (pptv)[a]	180	324	451	122	183	145
$F\text{–}NO_x \times 10^{13}$ (molecule m^{-2} s^{-1})[b]	–	0.94	3.10	1.30	–	0.66
ΔNO_x (pptv)[b]	–	-63	−153	−51	–	−32
$NO_2 : NO$[a]	1.3	1.5	2.8	2.0	1.1	0.60
T_{air} (°C)	−34.5	−34.5	−31.0	−27.4	−31.5	−30.9
wind speed ($m\,s^{-1}$)	6.3	3.6	2.5	3.8	2.4	2.2
K_h ($m^2\,s^{-1}$)	–	0.046	0.049	0.080	–	0.043
h_z (m)[c]	–	19	20	36	6–59	18–25
$J_{NO_3^-} \times 10^{-8}$ (s^{-1})	–	–	2.93	2.68	–	–
SZA (°)	69.7	68.1	67.6	67.9	67.6	67.9
column O_3 (DU)	301	294	272	297	311	309
$NO_{3\,skin\,layer}^-$ ($ng\,g^{-1}$)[d]	513	764	1090	439	866	1212
O_3 (ppbv)	34.2	35.7	31.9	21.1	24.6	22.6

[a] At 1 m above the snow surface.
[b] Based on concentrations at 1.0 and 0.01 m above the snow surface.
[c] Model estimates.
[d] From daily sampling of the top 0.5 cm of snow.

ACPD
14, 31281–31317, 2014

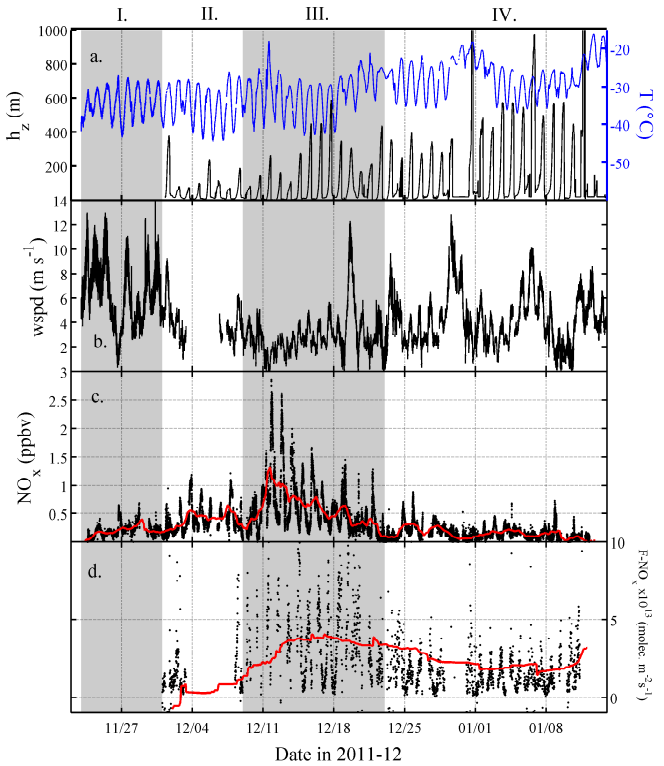

Figure 1. Meterorology and NO_x observations at Dome C in summer 2011–2012 (highlighted periods I.–IV. as referred to in text and Table 2): **(a)** air temperature (T) at 1.6 m and modeled mixing height (h_z) (Gallée et al., 2014), **(b)** wind speed (wspd) at 3.3 m **(c)**, 1 min averages of NO_x mixing ratios at 1 m (red line is 1 day running mean) and **(d)** 10 min averages of observational estimates of NO_x flux (F_{NO_x}) between 0.01 and 1 m (red line is 14 day running mean).

ACPD
14, 31281–31317, 2014

Atmospheric nitrogen oxides during OPALE

M. M. Frey et al.

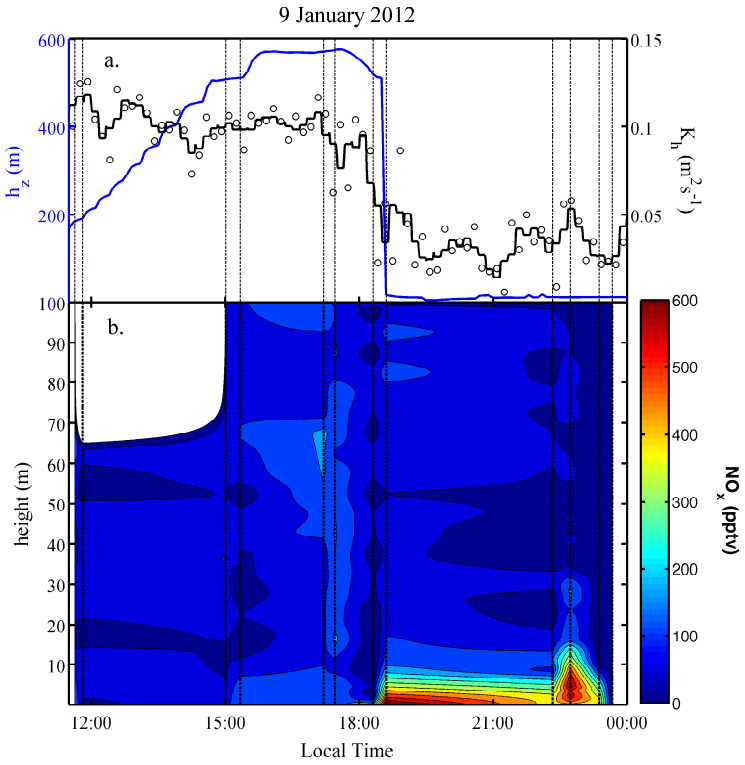

Figure 2. Balloon profiles (vertical dashed lines) from 9 January 2012: **(a)** modelled mixing height h_z (10 min running mean) and observed turbulent diffusion coefficient of heat K_h (10 min averages and 30 min running mean) at 1 m. **(b)** interpolated vertical profiles of NO_x mixing ratios with contour lines representing 60 pptv intervals. The lower 100 m appear well mixed during the day, while after collapse of the convective boundary layer in the early evening snow emissions of NO_x are trapped near the surface causing a strong increase in mixing ratios near the ground.

ACPD
14, 31281–31317, 2014

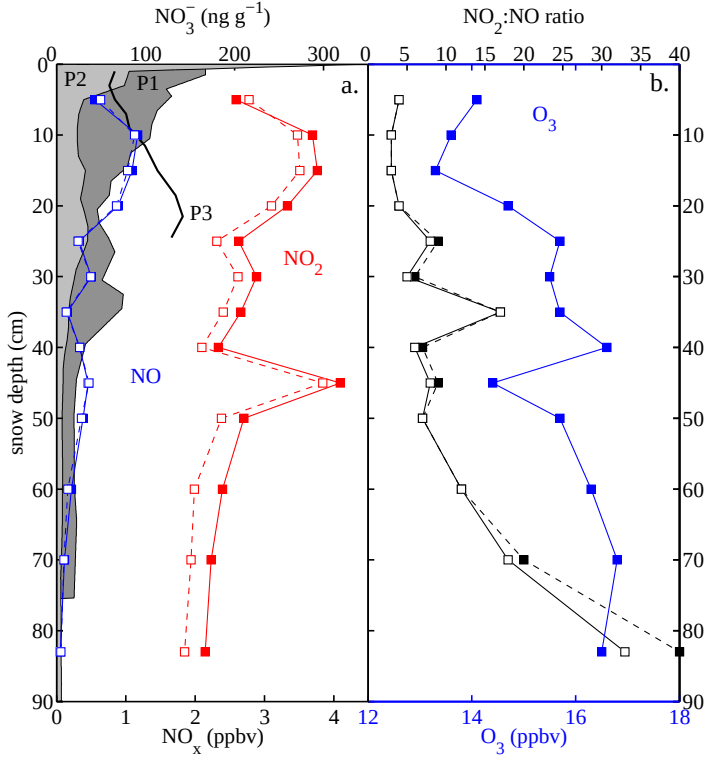

Figure 3. Firn air mixing ratios of NO_x **(a)** and O_3 **(b)** observed on 12 January 2012. Symbols represent 30 min averages and dashed lines are results from a 50 m long intake line. Shown are also NO_3^- concentrations in snow at 100 m (P1) and 5 km (P2) distance from the lab shelter as well as from under the firn probe (P3).

ACPD
14, 31281–31317, 2014

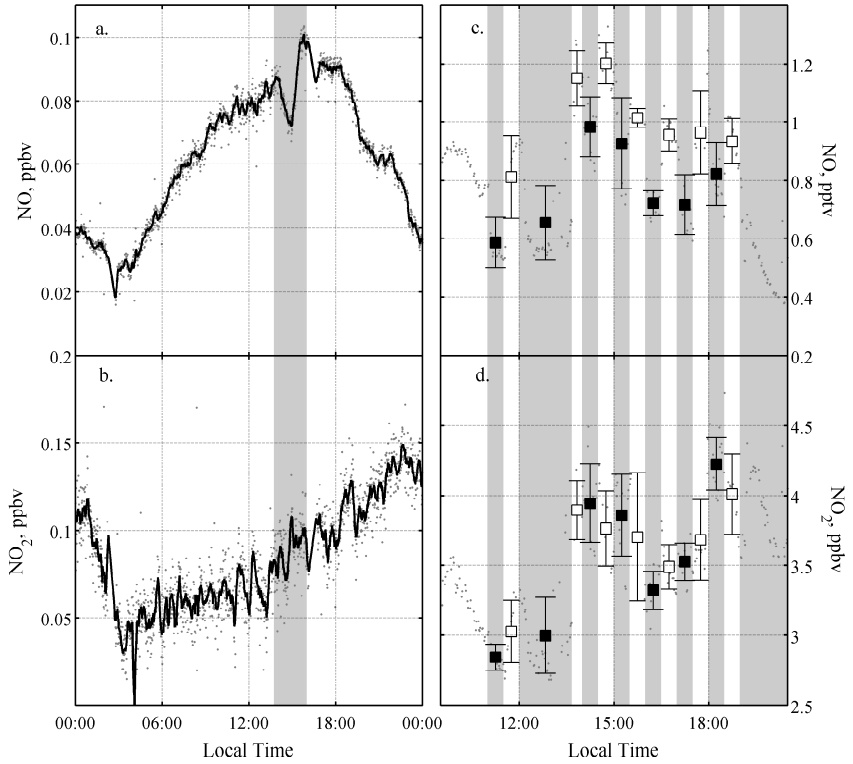

Figure 4. The impact of rapid changes in incident solar radiation on atmospheric NO_x mixing ratios (1 min values). **(a–b)** ambient concentrations at 1 m during a partial solar eclipse on 25 November 2011 (shaded area) with black lines representing the 10 min running mean. **(c–d)** firn air concentrations at 10 cm depth during a shading experiment using UV-filters on 11 January 2012. Square symbols and error bars represent interval averages and SD, respectively. Shaded areas and filled squares indicate time periods when the UV filter was in place.

ACPD
14, 31281–31317, 2014

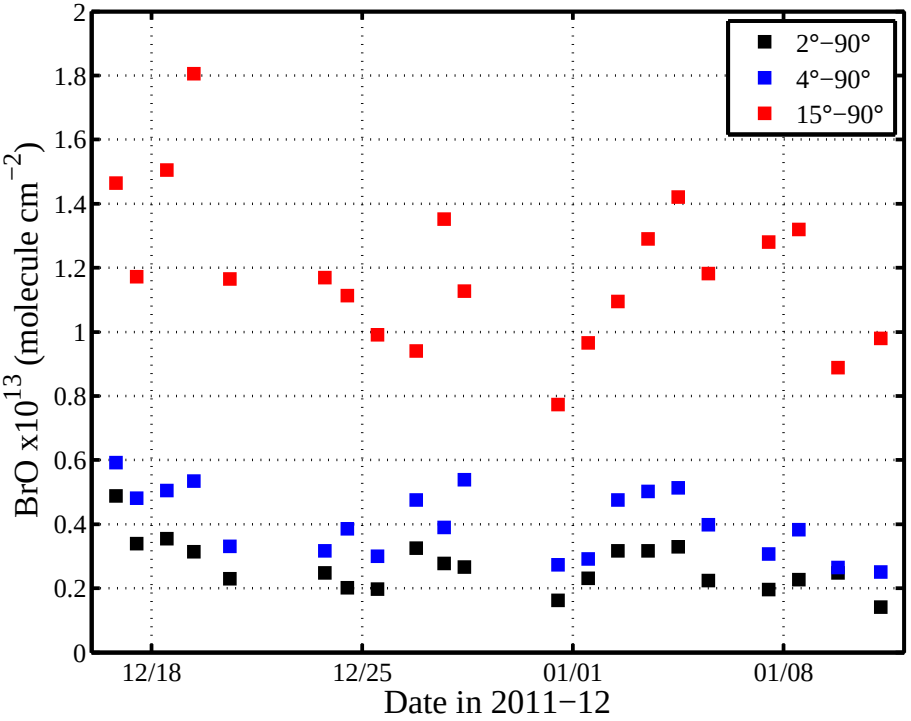

Figure 5. Median daily values of MAX-DOAS BrO vertical amounts from Dome C during sunny days or part-days only, after subtracting zenith amounts (see text). Reference spectrum from near-noon on 18 December until 6 January, then from near noon on 7 January. The apparently larger vertical amounts at higher elevations show that much of the BrO is in the free troposphere.

ACPD
14, 31281–31317, 2014

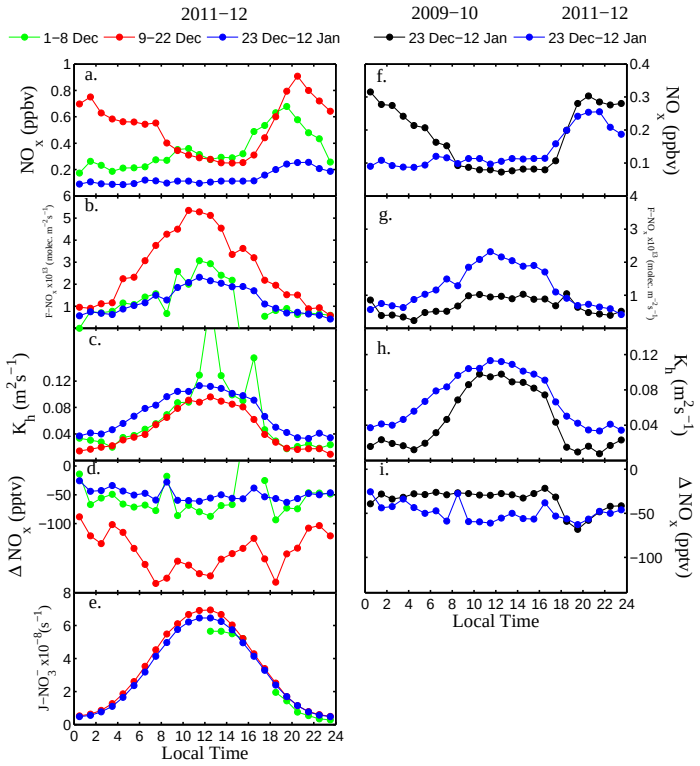

Figure 6. Observed median diurnal cycles during selected intervals in 2011–2012 **(a–e)** (referred to as periods II.–IV. in Table 2, Figs. 1, 7) and 2009–2010 **(f–i)**. Shown are NO_x mixing ratios at 1 m **(a, f)**, NO_x flux (F-NO_x) between 0.01 and 1 m **(b, g)**, the turbulent diffusion coefficient of heat (K_h) at 1 m **(c, h)**, the difference in NO_x mixing ratios (ΔNO_x) between 1.0 and 0.01 m **(d, i)**, and the 2π downwelling nitrate photolysis rate coefficient ($J_{NO_3^-}$) **(e)**. Note comparable observations of $J_{NO_3^-}$ are not available from 2009–2010.

ACPD
14, 31281–31317, 2014

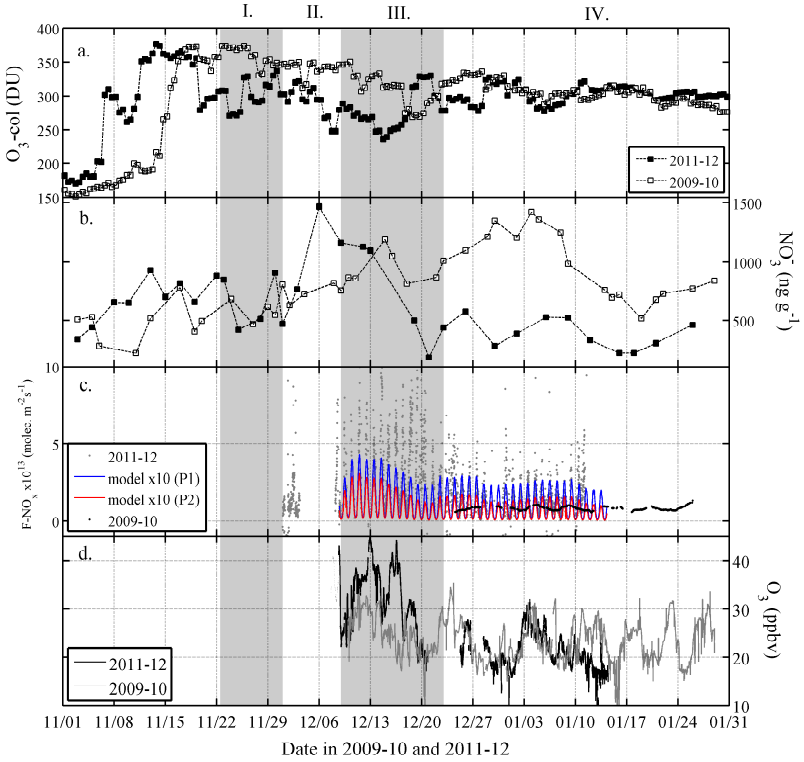

Figure 7. (a) Total column O_3 above Dome C. **(b)** NO_3^- concentrations in the skin layer of surface snow (top 0.5 cm). **(c)** observational estimates of NO_x flux (F_{NO_x}) between 0.01 and 1 m (10 min averages) and modelled F_{NO_2} (multiplied by 10) based on NO_3^- in the skin layer and depth profiles observed at 100 m (P1) and 5 km (P2) distance from the lab shelter (see Fig. 3a); the 1 day running mean of F_{NO_x} during 2009–2010 is shown for comparison (from Frey et al., 2013) **(d)** atmospheric O_3 mixing ratios. Highlighted periods I.–IV. as referred to in text and Table 2.

ACPD
14, 31281–31317, 2014